EPJ manuscript No.
(will be inserted by the editor)

First operation of an ALICE OROC operated in high pressure Ar-CO_2 and Ar-CH_4

A. Ritchie-Yates[1] [a], A. Deisting[1] [b], G. Barker[2], S. Boyd[2], D. Brailsford[3], Z. Chen-Wishart[1], L. Cremonesi[4], P. Dunne[5], J. Eeles[1], P. Hamilton[5], A.C. Kaboth[1], N. Khan[5], A. Klustová[5], J. Monroe[1], J. Nowak[3], P. Singh[4], A.V. Waldron[4], J. Walding[1], L. Warsame[5], M.O. Wascko[5], and I. Xiotidis[5]

[1] Royal Holloway, University of London, United Kingdom
[2] University of Warwick, United Kingdom
[3] Lancaster University, Bailrigg, Lancaster, United Kingdom
[4] Queen Mary, University of London, United Kingdom
[5] Imperial College London, United Kingdom

Received: date / Revised version: date

Abstract New neutrino-nucleus interaction cross-section measurements are required to improve nuclear models sufficiently for future long baseline neutrino experiments to meet their sensitivity goals. A time projection chamber (TPC) filled with a high-pressure gas is a promising detector to characterise the neutrino sources used for such experiments. A gas-filled TPC is ideal for measuring low-energy particles, which travel further in gas than in solid or liquid detectors and using high-pressure increases the target density, resulting in more neutrino interactions.

We examine the suitability of multiwire proportional chambers (MWPCs) from the ALICE TPC for use as the readout chambers of a high-pressure gas TPC. These chambers were previously operated at atmospheric pressure. We report the successful operation of an ALICE TPC outer readout chamber (OROC) at pressures up to 4.2 bar absolute (barA) with Ar-CH_4 mixtures with a CH_4 content between 2.8 % and 5.0 %, and so far up to 4 bar absolute with Ar-CO_2 (90-10).

The charge gain of the OROC was measured with signals induced by an ^{55}Fe source. The largest gain achieved at 4.2 bar was $(29 \pm 1) \cdot 10^3$ in Ar-CH_4 with 4.0 % CH_4 with an anode voltage of 2975 V. In Ar-CO_2 with 10 % CO_2 at 4 barA, a gain of $(4.2 \pm 0.1) \cdot 10^3$ was observed with anode voltage 2975 V. We extrapolate that at 10 barA, an interesting pressure for future neutrino experiments, a gain of 5000 in Ar-CO_2 with 10 % CO_2 (10000 in Ar-CH_4 with $\sim$4 % CH_4) may be achieved with anode voltage of 4.6 kV ($\sim$3.6 kV).

PACS. XX.XX.XX No PACS code given

Acknowledgements

The authors gratefully acknowledge the help of Ian Murray with lab equipment, gas orders and support during the operation of the detector, Richard Elsom, Paul Bamford and Ian Higgs with the production of detector parts and Chilo Garabatos on behalf of the ALICE Collaboration for sending the OROC used in this paper to the UK. This project has received funding from the European Union's Horizon 2020 Research and Innovation programme under grant agreement No 101004761 and an EU Horizon 2020 Marie Skłodowska-Curie Action. This research was furthermore funded in part by Science and Technology Facilities Council grant number ST/N003233/. We thank UKRI for supporting several authors of this paper.

[a] Corresponding author: A.R.-Y. 0009-0009-1230-4558 harrison.ritchie-yates.2013@live.rhul.ac.uk

[b] Now at: Johannes Gutenberg-Universität Mainz, Institut für Physik, 55128 Mainz (DE)

1 Introduction

A time projection chamber (TPC) filled with a high pressure gas is a promising detector to characterise interactions from high-intensity neutrino sources, *e.g.* the neutrino beams of future long-baseline neutrino experiments such as the Deep Underground Neutrino Experiment (DUNE) and Hyper-Kamiokande (HK). Using this kind of detector as part of a near detector complex provides substantial robustness to oscillation analyses, for example, as studied in the DUNE near detector (ND) conceptual design report [1].

High resolution measurements of neutrino-nucleus interaction cross-sections are required as an input parameter to improve the cross section models used for neutrino oscillation analyses. In the near future, the uncertainties related to these models will be the main contribution to the systematic uncertainties of oscillation analyses so they need to be reduced in order for future neutrino oscillation experiments (like DUNE and HK) to reach their sensit-

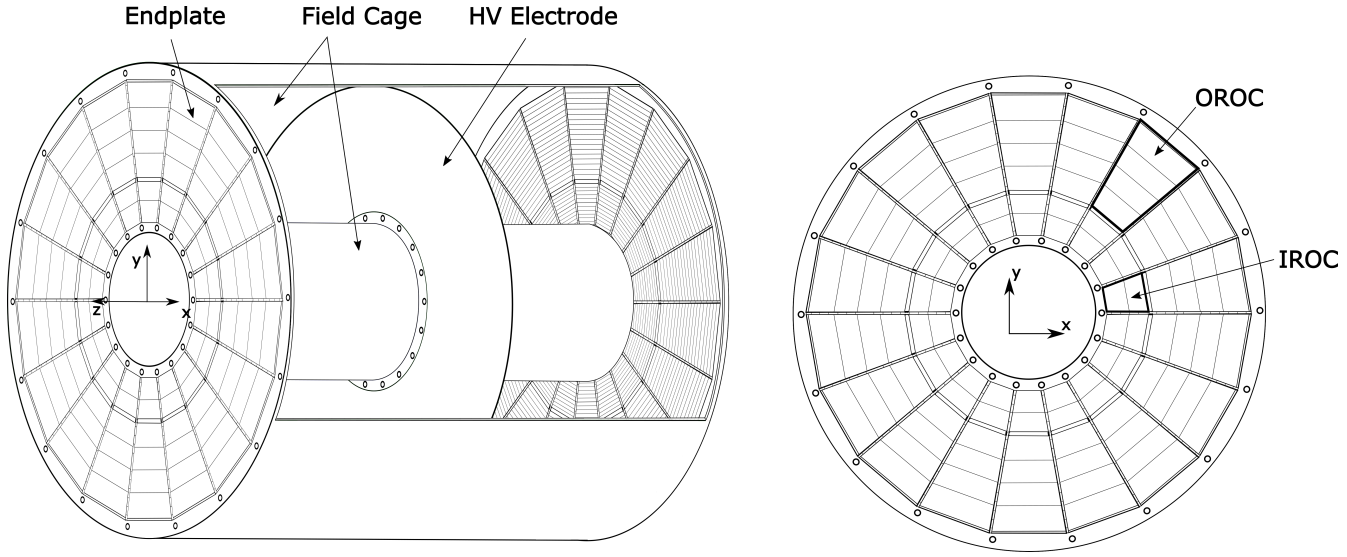

Figure 1: Schematic of the ALICE TPC. The TPC features a central drift electrode. Readout chambers are arranged in two endplates; each endplate has 18 sectors of one OROC and one IROC, for a total of 36 readout chambers per endplate. Further tracking detectors and the beam pipe are enclosed in an inner cylinder.

ivity goals [2]. Current experiments like T2K and NOνA also suffer from mismodelling of neutrino-nucleus interactions [3, 4]. Neutrino interactions with nuclei are measured by their final state particles, which are ejected from the nucleus after an interaction; measuring all (charged) final state particles requires measuring protons and pions with a low kinetic energy of a few 10 MeV [1]. A gas filled TPC is ideal for this task. A gas TPC can grant coverage over the full solid angle and, since particles will travel further in a gas medium than they will through a liquid, a gas TPC can measure lower momentum particle tracks than can be measured with a liquid filled TPC. Since neutrinos interact very rarely, even with the MW-scale beams of future neutrino experiments it would be necessary to use a high-pressure gas to increase the target density and allow more scattering events to be recorded.

The ALICE TPC [5] has been recently upgraded with new readout chambers [6], allowing for continuous readout. Consequently, the previously used multiwire proportional chambers (MWPCs) have become available and we will study in this paper how they could be used at a future long-baseline neutrino experiment's ND. These chambers are the appropriate size for a future long-baseline detector, and provide a useful platform for research and development of high pressure TPC (HPTPC) readout technology and test stands. As the ALICE TPC is operated at atmospheric pressure, these MWPCs need to be tested at higher pressures. To achieve the millions of neutrino interactions needed to constrain neutrino cross-sections, approximately a tonne of gas would be needed. Achieving this mass in the volume of the ALICE TPC would require a pressure of 10 bar absolute (barA).

This paper reports on gas gain measurements with an ALICE outer readout chamber (OROC) at the UK high pressure test stand operated at Royal Holloway, University of London (RHUL). In the remainder of this section we will introduce the ALICE TPC and the design of the OROC (Sec. 1.1). The UK high pressure platform will be presented in Section 1.2. Section 2 describes how these components form the full test set-up and the measurement procedure; and in Section 3 the analysis is detailed. Results are given in Section 4, showing the operation of the OROC at pressures up to 4.2 barA with different gas mixtures with argon predominance (Ar-CH_4 and Ar-CO_2). We conclude this paper with Section 5.

1.1 ALICE TPC multiwire proportional chambers

ALICE [7, 8] – short for *A Large Ion Collider Experiment* – is an experiment dedicated to the study of the quark gluon plasma in heavy-ion collisions at CERN's LHC. The ALICE TPC [5] is the experiment's main tracking and particle identification detector and is optimised to measure the trajectories of charged particles and their specific energy loss in the high multiplicity environment of Pb-Pb collisions. The original TPC has been designed to track up to 8000 charged particles per rapidity unit per event at a trigger rate of 300 Hz. It has so far been operated at atmospheric pressure with Ne-CO_2-N_2 (90-10-5) – here and throughout the paper the numbers in brackets denote the mixing ratio by volume – and Ar-CO_2 (88-12).

A sketch of the ALICE TPC is shown in Figure 1. It follows a cylindrical design of 5 m length and 5.16 m diameter, with a cylindrical cut out of 157.6 cm diameter at the centre. The ROCs (readout chambers) sit on the end-plates facing the drift cathode at the centre of the TPC. There are 18 inner readout chambers (IROCs) and OROCs per end-plate. In LHC run 3, ALICE will take data at a rate of 50 kHz in Pb-Pb collisions and it will examine every event recorded at that rate. For this reason, the ALICE TPC was upgraded with new readout cham-

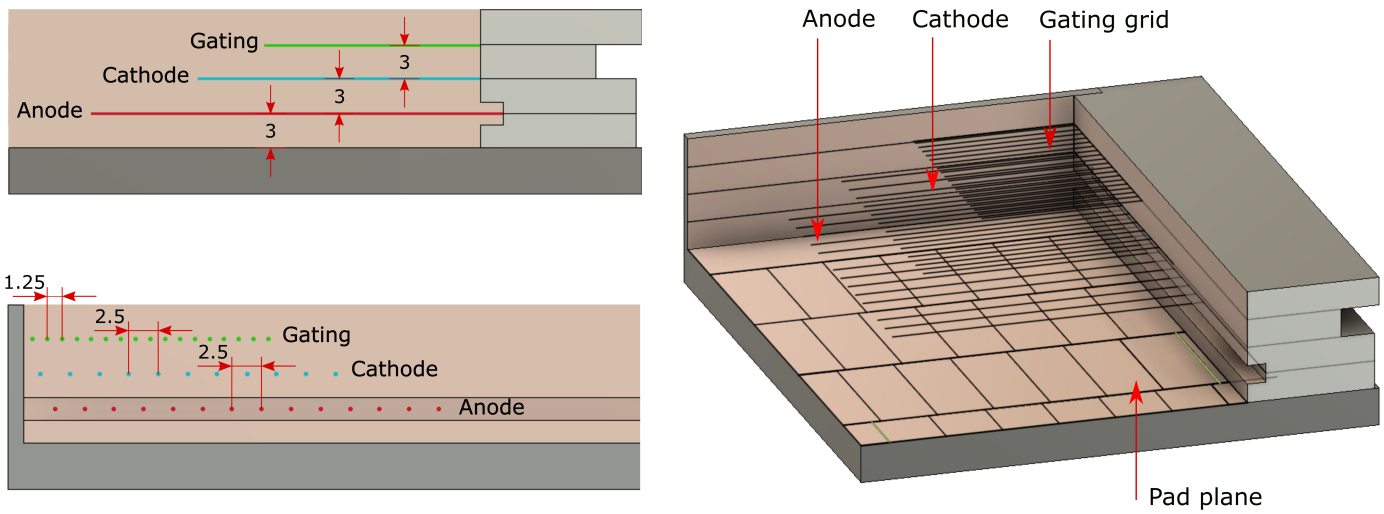

(a) (b)

Figure 2: Geometry of the OROC wire- and pad plane layout. (a) Cross section through the ROC perpendicular (top) and parallel (bottom) to parallel sides of the ROC's trapezoid shape (see Fig. 3) Distances are in mm. (b) A 3D view of one of the ROC's corners.

bers allowing for continuous readout of the TPC [6]. This has made all ALICE TPC MWPCs available to be used by a different experiment, so they could be re-purposed for use in a high-pressure TPC.

In Figure 2 the wire geometry of an OROC is shown. There are three wire planes: the anode wire grid, the cathode wire grid and the gating grid, where the latter separates the TPC drift volume from the actual ROC. The trapezoidal active area (Fig. 3) of an OROC measures 45.8 cm and 86 cm on the small and on the long end, respectively, defining also the location of the shortest (43.4 cm) and longest (83.6 cm) wire length. Wires run in parallel to the parallel sides of the trapezium. The length of the chamber perpendicular to the wires is 114 cm. The spacing between each plane of wires is 3 mm and the anode wires sit 3 mm above the pad plane. The gating grid wires are 75 µm diameter copper beryllium wires with a pitch of 1.25 mm. An offset voltage of $+\Delta V_{\mathrm{gg}}$ or $-\Delta V_{\mathrm{gg}}$ can be applied on every other wire in addition to the constant gating grid wire voltage V_{gg}, thus creating an electric field configuration in which electrons from the drift volume and ions from the inside of the ROC end up on the gating grid wires and do not cross the grid. The cathode wire grid is also made from copper beryllium wires of 75 µm diameter. Their pitch is 2.5 mm, staggered with respect to the gating grid wires. The particular OROC we used for the studies in this paper was never part of the ALICE TPC, but was used for tests by the ALICE collaboration. As such it has a feed-through, which allows the cathode wire grid to be biased or read out. In the ALICE TPC the cathode wires were held at ground potential. The anode wires are 20 µm in diameter. Like the cathode wires, their pitch is 2.5 mm and they are staggered with respect to both the cathode and gating wire grid. The first two and last two anode wires, called edge wires, are 75 µm in diameter. The anode wires are designed for high voltage (HV) and so are made of gold-plated tungsten, which has a higher strength than the copper beryllium used for the other wires. The upper voltage limit which the anode wires can maintain without sustaining damage has not been determined, but the OROC has been operated with anode voltages up to 3000 V.

Ionization electrons are produced in the drift region by charged particles or photons and drift to the amplification region in the ROC under the influence of the electric field produced by the TPC's HV electrode and the gating grid wires. In the ROC these electrons undergo avalanche charge multiplication around the anode wires, inducing charge on the pads. The pad plane is made up of 9984 pads of two different pad sizes. The size of the outer 4032 pads (32 pad rows) is $6 \times 15\,\mathrm{mm}^2$, the size of the inner 5952 pads (64 pad rows) is $6 \times 10\,\mathrm{mm}^2$. Outer and inner refers to the pad rows closer to the longer and shorter end of the OROC, respectively. Figure 3 indicates the border between the rows of different pad sizes. The pads are grouped in groups of 21 or 22 pads and are connected to sockets on the back of the OROC. Diagrams of the pads, groups, and sockets are shown in Figure 3. In the ALICE TPC, the position of the original ionisation electrons in the drift volume can be determined from the pad signals, which determine the location in x and y. The third coordinate is determined by the arrival time of the charge at the ROC, projecting back to a t_0 given by a trigger.

The design of the similar, albeit much smaller IROC can be found in Ref. [5], together with additional information on the ROCs and the ALICE TPC.

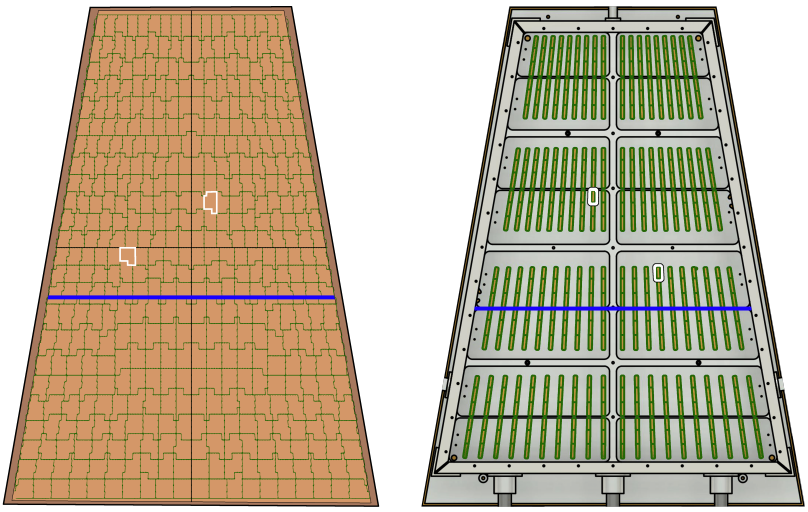

(a) (b)

Figure 3: Diagrams of (a) the pad-plane side of the OROC, showing the wires and pad plane and (b) the connector side of the OROC showing the sockets used for readout and grounding of pads. The pad plane is made up of 96 rows of two different pad sizes, the boundary between the upper 64 rows of $6 \times 10\,\mathrm{mm}^2$ pads and the lower 32 rows of larger, $6 \times 15\,\mathrm{mm}^2$ pads is indicated by the blue line in each diagram. The pad plane is segmented into groups of 21 or 22 pads, which can be read out from the sockets on the back of the OROC (see Figure 7). The groups and their corresponding sockets have been outlined in green and the two pad groups used for readout for the studies in this paper are outlined in white in each diagram.

1.2 UK high pressure platform

The UK high pressure test stand operated at RHUL allows for the testing of TPC technology in the pressure range from sub-atmospheric pressure up to 4 barG, where the unit barG is used to indicate gauge pressure. It features a high pressure vessel (*cf.* Fig. 4) with an inner diameter of 140 cm, which is to our knowledge the only vessel which can be used to test ROCs as large as an OROC at pressures higher than atmospheric pressure. A detailed description of the test stand can be found in Ref. [9]. The cylindrical vessel with domed ends is made from stainless steel (type 304L) and has a total volume of $1472\,\mathrm{dm}^3$. One of the ends can be removed to access the inside of the vessel. A system of three rails allows a TPC with a drift length of more than 50 cm to be mounted, depending on the width of the TPC's readout structure. The vessel has various feed-throughs to attach HV and signal lines, and to supply the vessel with gas or evacuate it. The vessel at RHUL is connected to a gas system which allows for evacuation to 1×10^{-6} barA, and gas mixing by partial pressures up to 5 barA from 4 inputs.

2 Experimental set-up and measurement procedure

For the studies detailed in this paper, the TPC used is mounted inside the high pressure vessel at RHUL on three Delrin rails, 600 mm in length. The drift volume in this set-up is created by the same drift cathode and field cage as described in Ref. [9]. The drift cathode is a steel mesh ring with a radius of 1120 mm made from 25 lpi (lines per inch) mesh of 27 µm diameter wires. The field cage is made of 8 copper rings with an inner diameter of 1110 mm. We define a coordinate system such that the pad plane of the OROC is in the xy plane. The coordinate along the remaining axis (the TPC symmetry axis) is then z. Each field cage ring has a width of 10 mm in (z) and the distance between each ring in z is 25 mm, yielding a total field cage length of 255 mm. These field-shaping rings are connected by a series of $3\,\mathrm{M}\Omega$ resistors to reduce the potential between each ring. Resistors of the same resistance are used to connect the first ring to the drift electrode and the final ring to ground.

The shape of the amplification region (*i.e.* the OROC) is trapezoidal but the drift region is cylindrical. To account for this transition, three plates are mounted in a plane between the drift region and amplification region to cover the area of the drift region not covered by the OROC, thus terminating the field lines there. This termination plane is steel with 1 mm thickness and it is also mounted on the same Delrin rails supporting the TPC. A diagram of the TPC is shown in Figure 5 and a photo of the set-up in Figure 6.

The total drift distance from the drift electrode to the OROC anode wires is 336 mm. For the data presented in Section 3 the TPC was operated with a drift cathode voltage of −16 kV and hence a drift field of $-476\,\mathrm{V\,cm}^{-1}$. The gating grid voltage V_{gg} was adjusted to the equipotential at the position of the gating grid, *i.e.* −143 V for the drift cathode voltage mentioned before.

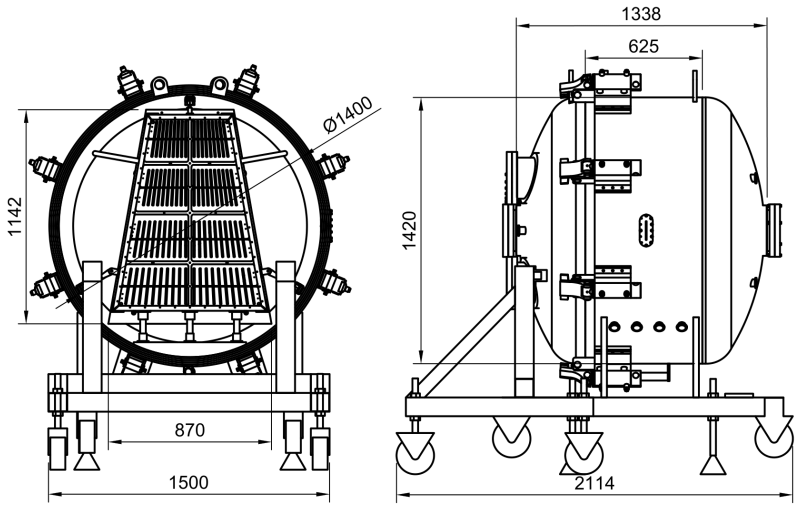

Figure 4: Schematic drawings of the HPTPC pressure vessel, shown are the front (left), and side (right) views. The front view (cutaway) also shows the OROC support frame mounted on the vessel rails.

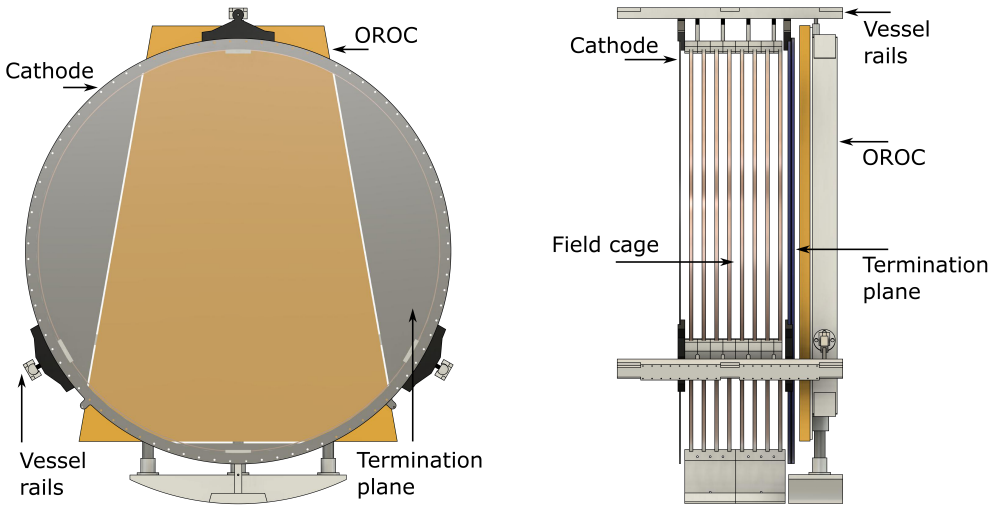

Figure 5: Three dimensional CAD rendering of the TPC, (a) view from the back of the vessel and (b) side view, showing the drift cathode, field cage, terminator plane, and OROC support frame, as well as the rails on which the TPC is mounted in the pressure vessel.

2.1 Charge readout hardware

The measurements taken for this paper investigate the response of the test OROC to an ^{55}Fe source. The source is suspended in the vessel close to the OROC wires, so that only a small part of the OROC can see the source; for this reason, we read out only a small section of the OROC pad plane. The pad plane is segmented into 468 groups of 21 or 22 pads, as indicated in Figure 3. To group pads for readout or for shortening to ground, we use *shorting cards* (*cf.* Fig. 7). These cards connect to the sockets on the back of the OROC and each connect three pad groups (21, 22 and 21 pads each) into one channel. Using one third of the connections of a shorting card, one group of 21 inner ($6 \times 10\,\mathrm{mm}^2$) pads near the ^{55}Fe source are grouped and read out together as a single channel. We refer to this channel as the signal channel. To measure only background signals (cosmic radiation) and noise, another card is used in the same way to readout another pad group (21 inner pads) from a part of the pad plane away from the source. This channel is referred to as the background channel. The positions of these two pad groups are shown in Figure 3, all other pads are connected to ground.

The signals from each channel are amplified by CREMAT CR-111 charge sensitive pre-amplifiers mounted in CREMAT CR-150-R5 evaluation boards. The pre-amplifiers have gains of $0.121\,\mathrm{mV\,pC^{-1}}$ (signal channel) and $0.128\,\mathrm{mV\,pC^{-1}}$ (background channel), and nominal out-

put waveforms with a 3 ns rise-time and 50 µs decay. Full specifications of the pre-amplifiers are given in Ref. [10].

When charge is induced on the OROC pad plane, the output from the preamplifier is a pulse with a height proportional to the induced charge. Following pre-amplification, a low-pass filter is used to reduce noise and the output waveforms are then digitised by a CAEN N6730 digitiser with 2 V dynamic range and a 500 MHz sampling frequency. The shape of typical signals recorded by the digitiser are described and diagrammed in section Section 3.

2.2 Measurement procedure

For each gas mixture and pressure, several voltage settings with varying anode voltage (V_a) but the same gating grid voltage (V_{gg}) and drift cathode voltage (V_d) are used. As we measured with an ^{55}Fe source, space charge distortions are of no concern and all gating grid wires were supplied with the same V_{gg} without any additional potential, operating the chamber with the gating grid constantly open. The voltage at the gating grid wires is optimised to match the potential given by the drift field 3 mm above the OROC's cathode wires ($\frac{-476\,\mathrm{V\,cm^{-1}}}{3\,\mathrm{mm}} = -143\,\mathrm{V}$). In the test setup in the pressure vessel the edge wires are connected to ground, the rest of the anode wire grid is biased with a HV V_a. The anode grid is split into 7 HV regions, which are all biased by the same power supply (PS) channel. A protection resistor of 3 MΩ is installed between each region at the point where the supply lines are soldered together and from there fed to the PS.

At each setting, several thousand waveforms are acquired where the data acquisition (DAQ) triggers either on the signal or background channel. The trigger thresholds are optimised to be just below the pulse's baseline, allowing for noise events to be recorded, too. During data taking the digitiser is prevented from saturating by adjusting the trigger threshold in cases where *e.g.* a baseline change leads to a saturation of the DAQ with noise signals. If the readout is triggered by either the signal channel or background channel, both channels are read out. The recorded waveforms include a pre-trigger region in which one quarter of the waveform's samples are data recorded before the sample where the trigger condition is met (*pre trigger*, Fig. 8a). Typically, waveforms are recorded for 300 µs including a pre-trigger time of 75 µs.

After it is deemed that enough signals have been recorded for one setting, V_a is changed and data recorded at the new configuration. The number of signals recorded at each voltage setting was chosen so to result in an amplitude spectrum which contains a peak that can easily be discerned by eye and fitted by the analysis described in section 3. After data cleaning, typically between 10-25 % of the recorded waveforms sit within the photopeak so, to this end, for the data taken with Ar-CO_2, between 4000 to 12000 waveforms were collected at each voltage setting. We observe that, with Ar-CH_4, the ratio of ^{55}Fe signals in the photopeaks to background signals due to (e.g.) cosmic radiation is lower than the ratio observed with Ar-CO_2 by a factor of ∼2.5. As possible reasons we examined the transversal diffusion, which is more than 3 times larger in Ar-CH_4 (96-4) than Ar-CO_2 (90-10) [11], and the number of electron-ion-pairs per track length of muons produced in the gas mixtures. The latter varies only by ∼5 % between the two mixtures over a $\beta\gamma$ range from 0.5 to 200 for muons [12]. The area of the diffusion clouds at 1 barA pressure is smaller than the pad area and smaller than the x-ray conversion length [11, 13]. Therefore we expect less fully contained events in the instrumented pads for the Ar-CH_4 mixtures, but not a general change of the fraction of ^{55}Fe events to other events. Given this, it is most likely that the source shifted slightly between the different data taking campaigns. In fact, we did open the detector and placed-and-replaced a source between the two campaigns. To account for the lower ^{55}Fe event count as compared to the cosmic radiation for the data taken with Ar-CH_4, more time was spent at each voltage setting, and between 12,000 to 36,000 waveforms were collected at each setting.

Ar-CO_2 data taking

For the measurement with Ar-CO_2, premixed Ar-CO_2 (90-10), grade N4, was used. This gas mix was used previously for the commissioning of the OROC for the ALICE TPC in 2009 [14]. Pressures measured start at 1 barA and are increased in steps of 0.25 barA up to 2.5 barA, and then in steps of 0.5 bar up to 4 barA – a total of 10 pressure settings. To investigate repeatability, the vessel was then evacuated to vacuum and filled again with the same gas mix and additional data was taken at the pressure settings 1.75 barA, 3 barA, 4 barA, and 4.5 barA. Table 1a lists the full list of Ar-CO_2 mixtures and pressures used. For the data taken with premixed Ar-CO_2 (90-10) gas mixture, the pressure was monitored in barG and converted to barA assuming an atmospheric pressure of 1 bar. To account for local variations in atmospheric pressure, these pressures are given with an error of 30 mbar.

Ar-CH_4 data taking

For the measurement campaign with Ar-CH_4, premixed Ar-CH_4 (90-10) (± 0.2 %) was used and diluted with pure Ar of grade N5.5. We aimed for a mixture with no more than 5 % CH_4 to avoid safety issues related to flammability. Starting from about 1 barA pressure, the gas mixture in the high pressure vessel was topped up with Ar-CH_4 (90-10) and Ar to increase the gas pressure in 0.5 bar to 1 bar steps. Increasing the pressure reduces the gain at a fixed voltage V_a, so the CH_4 fraction was slightly decreased during filling to increase the amplification factor. In Table 1b the Ar-CH_4 mixtures and pressures are listed in chronological order of the data taking. Since the Ar-CH_4 mixtures are mixed with the HPTPC gas system, measurements in barG with an assumed atmospheric pressure are no longer sufficient to provide an accurate measurement of the pressure and mixing ratio. Hence, for the data taking with Ar-CH_4, an additional pressure sensor was used to measure the ambient atmospheric pressure outside of the vessel and determine an accurate measurement of the gas pressure in barA. We estimate the un-

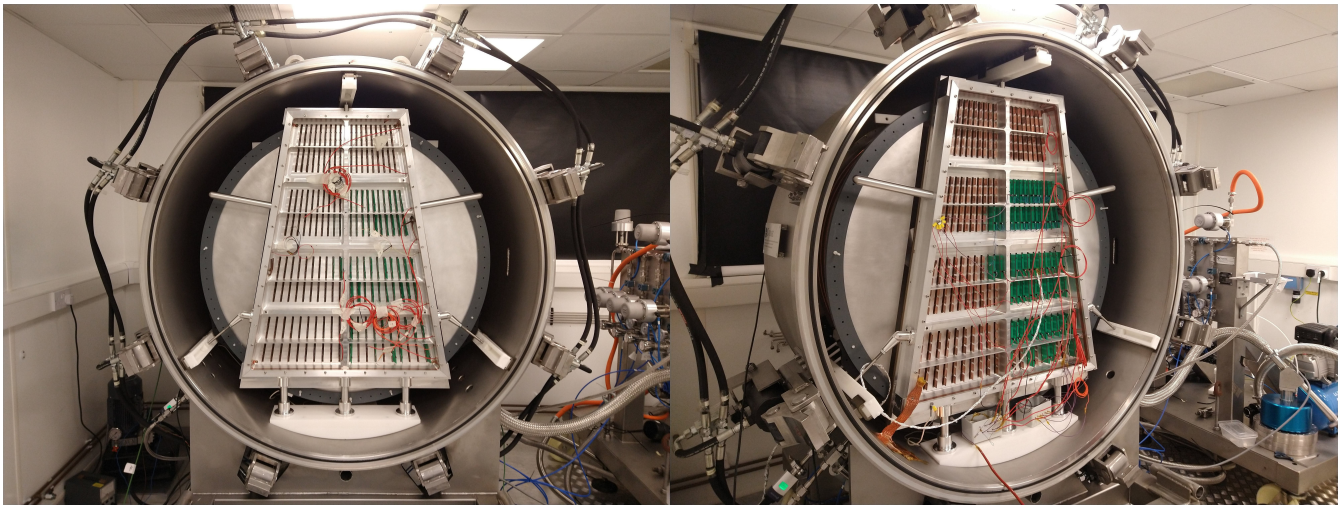

(a) (b)

Figure 6: Photos of the setup at RHUL. The TPC is mounted inside the pressure vessel on three white Delrin rails with the OROC supported by an aluminium frame. The gas system can also be partially seen to the right of both photos. Also visible in (b) are the HV connections for the anode and gating grid, and the shorting cards used for grounding and readout (see Figure 7).

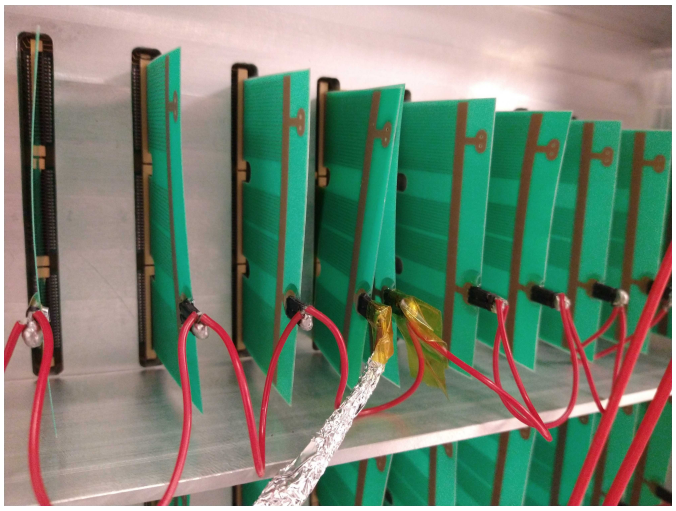

Figure 7: Shorting cards are used to group pads from three connectors at the back of the OROC into a single channel. The fourth card from the left is passivated on the lower two legs and connects with the upper leg only to the top connector. These 21 pads are opposite to the ^{55}Fe source and read out as the signal channel. The following card connects to the middle and lower connector in this row and the corresponding pad groups are connected to ground, as are all other pad groups which are not read out.

certainty to be less than 5 mbarA and we use this value throughout the paper for the Ar-CH_4 measurements. It is worth noting that the 3.49 barA mixture with 2.7 ± 0.2 % CH_4 could not be operated in a stable manner. Increasing the CH_4 content during the next mixture and pressure change allowed for a stable operation at higher pressure once again.

With Ar-CO_2, the minimum voltage setting at each pressure was chosen to be the lowest voltage at which the gas gain could be measured, i.e. the lowest voltage at which the ^{55}Fe photopeak is visible in the *Amplitude* spectrum above the trigger threshold. This is limited by electronic noise introduced in the readout chain. During the Ar-CH_4 data taking we started at lower voltages and thus recorded also data where no clear peak spectrum was visible. The maximum voltage setting at each pressure is decided by the onset of current draw on the anode wires (or discharges), since operating at voltages higher than this results in voltage drops on the anode and risks of damaging the wires. The point of onset of current draw

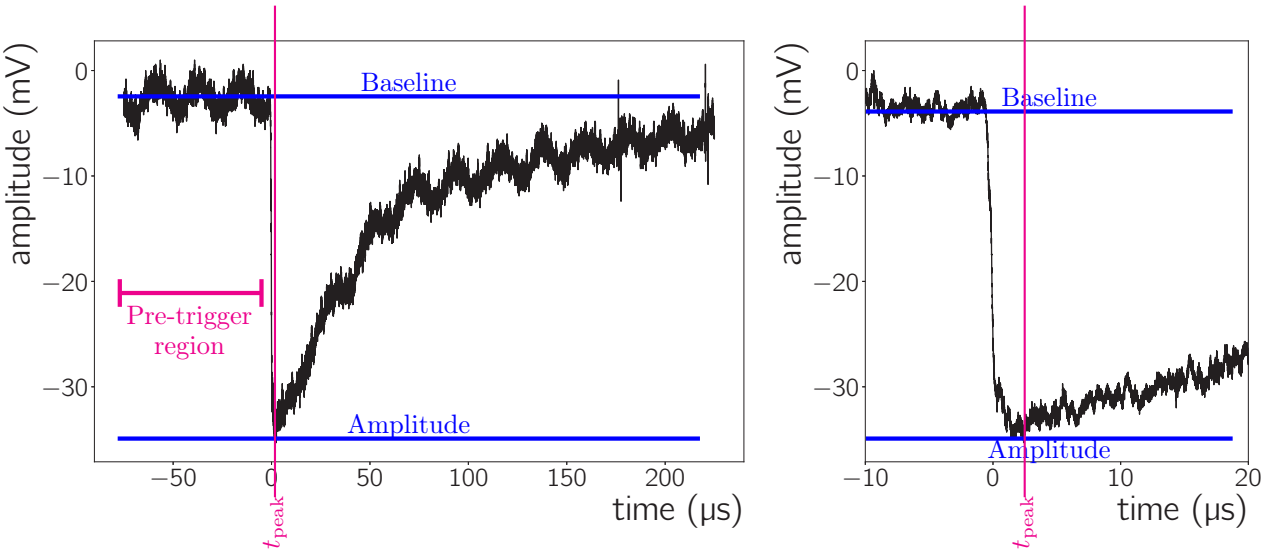

Figure 8: A typical waveform recorded for the studies in this paper: (a) The full waveform and (b) a zoom into the region of the peak. Lines indicate the values the analysis identified for the baseline (*Baseline*), the negative pulse amplitude (*Amplitude*), and the time sample where the sample with the highest amplitude was found (t_{peak}). The oscillations on top of the waveform are electronic noise.

can be increased if the anode wires are allowed to rest at high voltage for a period of time. This was used during the second Ar-CO_2 (90-10) fill to increase the maximum voltages at each setting. Table 1 details the minimum and maximum voltage settings used for each gas mixture and pressure setting. Note that for the pressure settings 1.25 barA and 1.5 barA in Ar-CO_2 we were still unfamiliar with the limits of the anode, so a lower maximum voltage of 1900 V was chosen, even when no current was observed. For later measurements all voltages below 3000 V were considered, however, we did not reach this limit with any gas mixture before observing currents on the anode wires.

3 Data analysis

Figure 8 shows a typical example of a pulse as recorded by the DAQ. For each waveform our analysis framework (described in Ref. [9]) calculates several characteristics. The most important ones for the analysis presented here are the *Baseline* value, the *Amplitude* value and the "peak-time", t_{peak}. The *Baseline* is the mean of all samples in the pre-trigger window, *i.e.* all samples for $t < 0$. The *Amplitude* corresponds to the pulse's negative amplitude: the sample with the lowest amplitude (A_{min}) is identified and the *Amplitude* value is calculated as $|A_{\text{min}} - \textit{Baseline}|$. Furthermore, the time at which A_{min} occurs is identified is t_{peak}.

3.1 Analysis of Amplitude spectra

Two cuts are applied on the calculated waveform parameters. The first cut requires the *Baseline* to be between −10 mV and 10 mV. This removes events triggered by baseline fluctuations caused by *e.g.* discharges. The second cut requires that $0.5\,\mu\text{s} < t_{\text{peak}}$. This cut on t_{peak} ensures that only pulses with a sensible shape are considered. We observe incidental noise peaks with a width of a few 100 ns, which are removed by this cut. Exponential smoothing is applied to the waveforms to counteract small fluctuations (RMS of ≤ 3 mV.) Each waveform is corrected according to:

$$V_i^{\text{smooth}} = \alpha_{\text{smooth}} \cdot V_i + (1 - \alpha_{\text{smooth}}) \cdot V_{i-1}.$$

Where V_i^{smooth} and V_i are the i^{th} sample (at time t_i) of the smoothed and raw waveform, respectively. The factor α_{smooth} is chosen as 0.005. A full discussion of the waveform smoothing as well as examples of smoothed waveforms can be found in Ref. [9]. Further analysis is then performed on histograms of *Amplitude* values for signals recorded at each voltage, gas mixture and pressure setting.

Figure 9 shows three *Amplitude* spectra for different V_{a} measured in Ar-CO_2 (90-10) at 1.75 barA. Comparing the signal and background channel spectra in these plots allows us to identify the background component due to cosmic radiation and the signal component from the ^{55}Fe x-rays. For spectra such as those shown in Figure 9, the photopeak of the ^{55}Fe source's x-ray emission and the Ar escape-peak are both visible. To extract parameters related to both of these peaks, the *Amplitude* spectra are

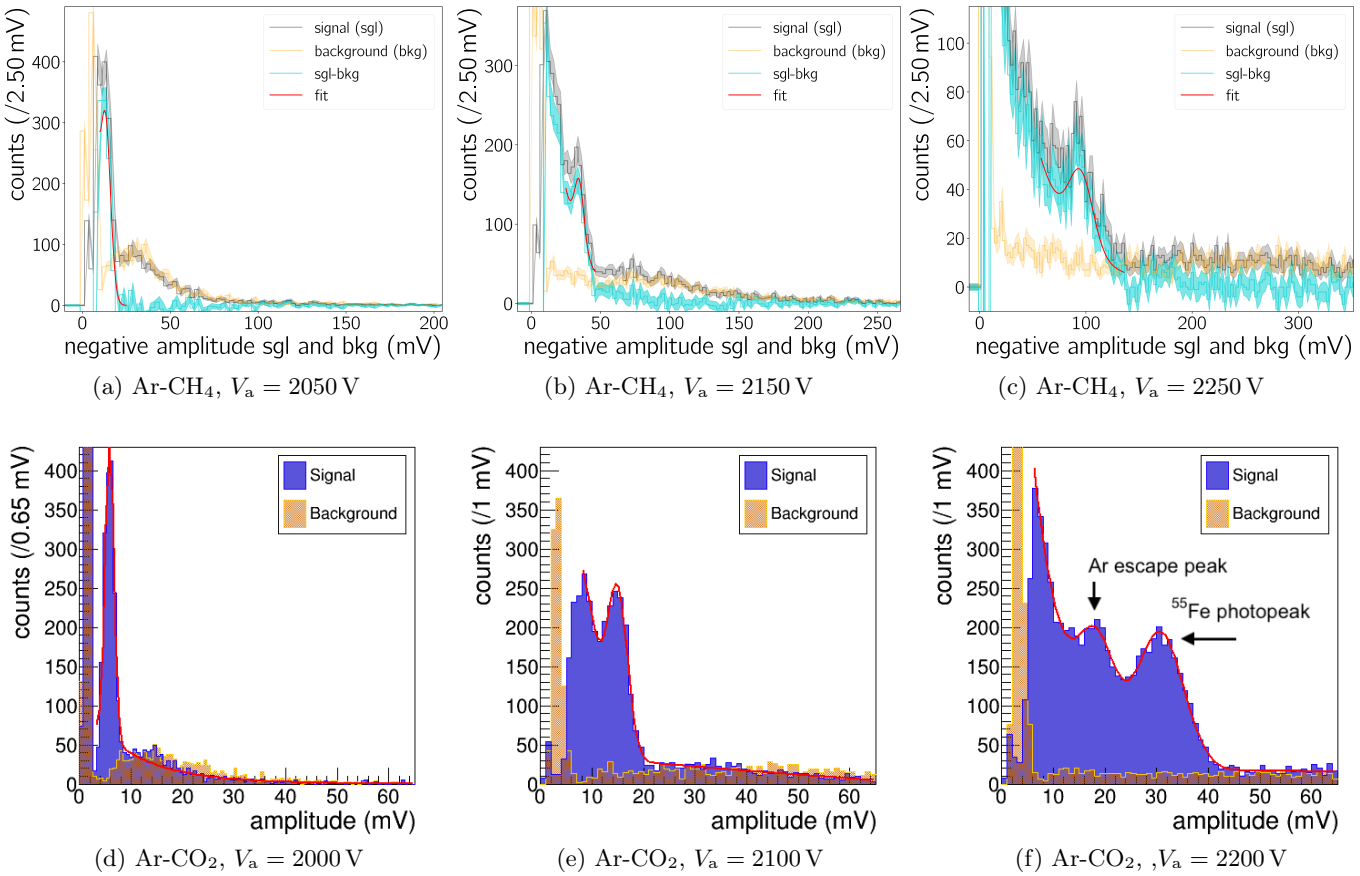

(a) Ar-CH_4, $V_a = 2050\,V$ (b) Ar-CH_4, $V_a = 2150\,V$ (c) Ar-CH_4, $V_a = 2250\,V$

(d) Ar-CO_2, $V_a = 2000\,V$ (e) Ar-CO_2, $V_a = 2100\,V$ (f) Ar-CO_2, ,$V_a = 2200\,V$

Figure 9: *Amplitude* spectra after cleaning cuts have been applied for data taken with Ar-CH_4 (95-5) at 1976 mbarA (top row) and with Ar-CO_2 (90-10) at 1750 mbarA (bottom row). Black (or blue) and orange histograms show the signal and background channels respectively. Shown are spectra for data taken with $V_{gg} = -143\,V$ and $V_d = -16\,kV$ ($E_d = -476\,V\,cm^{-1}$) and varying V_a as captioned. With higher V_a, the features of the amplitude spectra can be seen more clearly so, in (f), the photopeak from the ^{55}Fe source's x-ray emission as well as the lower amplitude Ar escape-peak are visible in the spectrum at 18 mV and 30 mV. These spectra are fitted with Eq. (2) for Ar-CH_4 data and Eq. (1) for the Ar-CO_2 data, the fits are shown in red for the appropriate fit ranges.

fitted with the function

$$f_1\,(Amplitude) = e^{p_0+p_1\cdot Amplitude} + p_2\cdot e^{-0.5\cdot\left(\frac{Amplitude-p_3}{p_4}\right)^2} + p_5\cdot e^{-0.5\cdot\left(\frac{Amplitude-p_6}{p_7}\right)^2} + p_8 \quad . \tag{1}$$

The first term of f_1 is an exponential function to fit the background and the second and third terms are Gaussian functions to fit the photopeak and escape-peak. A final constant, p_8, is added to fit the cosmic background tail. Figure 9 includes this function fitted to the signal channel's *Amplitude* spectra.

The escape-peak cannot be seen in all spectra. At lower OROC gas gains, the escape-peak has low enough amplitude such that it overlaps with the background exponential, and for higher observed OROC gas gains, the escape-peak is often washed out by the broadening of the peaks in the spectra. This is particularly true in the case of the Ar-CH_4 data, where we observe a worse energy resolution than for the Ar-CO_2 data and hence the ^{55}Fe peaks in the spectrum are broader and of lower amplitude, as will be shown in the next section, making them difficult to fit with (1). The challenges in fitting Eq. (1) to the Ar-CH_4 data can be addressed by tuning the start parameters and fit range. As we are however primarily interested in the position of the ^{55}Fe photopeak, a simplified approach was used for this analysis: the signal spectra are first subtracted by the background spectra (see Fig. 9, first row) and then fitted with the function:

$$f_2\,(Amplitude) = e^{p_0+p_1\cdot Amplitude} + p_2\cdot e^{-0.5\cdot\left(\frac{Amplitude-p_3}{p_4}\right)^2} \quad , \tag{2}$$

where only the ^{55}Fe photopeak is fitted. Doing so the signal amplitude values of the background channel are scaled by a factor $\frac{121}{128}$, to account for the difference in pre-amplifier gain between the two channels. Before subtracting background from signal spectrum, the background spectrum is normalised so that the its integral matches the in-

tegral of the signal spectrum outside of the larger boundary of the fit range. (Considering all fits made, this normalisation factor has a mean of 1.06 with a standard deviation of 0.27.) Using this approach of fitting f_2, *i.e.* Eq. (2), allows for automated fitting of all measured voltages, Ar-CH_4 mixtures and pressure settings.

Figure 10 shows the fit results for two of the free parameters of f_1 and f_2 for the fits to all Ar-CO_2 and Ar-CH_4 data. The χ^2 divided by the number of degrees of freedom was between 0.8 and 5.4 for all fits, and typically between 0.8 and 1.8. We omit all settings from the result plots in the next section in which no clear peak(s) related to the ^{55}Fe source can be seen in the spectrum.

4 Measurements and results

The peak position vs V_a measurements (Fig. 10a, Fig. 10b) demonstrate already one main aim of this work: An OROC can be operated at up to at least four times its design pressure. The exponential trends observed with increasing V_a for each gas mixture setting match the expectations given by the avalanche nature of the charge amplification. For a full characterisation of the chamber at high pressure, the gas gain and energy resolution are calculated from the fits to the *Amplitude* spectra discussed in Section 3. We also tested Ar-CH_4 mixtures with 4 % CH_4 content and 4.4 barA as well as 4.8 barA pressure, however no peak spectrum consistent with ^{55}Fe could be identified up to $V_\mathrm{a} = 2975$ V (Tab. 1b).

4.1 Energy resolution

Figure 11 shows the energy resolution ($\frac{\sigma_\mathrm{peak}}{\text{peak position}}$) as a function of anode voltage. For the most part the value is between 10 % and 25 %, 30 % for the highest gains measured. Better values than this have been obtained with OROCs, in ALICE this was as low as 6 % [5, 14]. The performance observed in this paper is likely explained by two differences in our set-up: The first is that the pre-amplifiers are located outside of the high pressure vessel, this means that all signals have to travel through a cable of significant length before they reach the pre-amplifiers. Figure 8 gives an idea of the noise encountered along the cable path. The second is the readout pad and the alignment of the ^{55}Fe source. The readout integrates signals from a group of 21 pads, increasing the detector capacitance when comparing to the ALICE TPC readout. Furthermore the source may not be perfectly aligned with the group of readout pads, enhancing the fraction of partial events. If the source is not perfectly aligned with respect to the readout pads, then the decrease in the x-ray's mean free path from 2.17 cm at 1 barA to 0.44 cm at 5 barA fewer x-rays will convert over the pads at higher pressure and a smaller fraction of events will be fully contained [13]. Comparing background and signal spectra, we observe the fraction of events attributed to the ^{55}Fe source to decrease at higher pressure. Since the general shape of the *Amplitude* spectra does not change as we increase the pressure, we are confident that we always have fully contained events within the readout pad, and since we are primarily concerned with the position of the peak in the *Amplitude* spectra, the effect of charge falling outside the signal pad group should not affect our gain measurement. Note that the measurements of energy resolution reported here refer specifically to the measurement with an ^{55}Fe source and are not a reflection of the ultimate energy resolution for tracked particles in the detector. The set-up has also not been optimised for its energy resolution.

4.2 Gas gain

The gas amplification factor, or gas gain, G_OROC, can be calculated as

$$\begin{aligned} G_\mathrm{OROC} &= \frac{q_\mathrm{amp}}{N_\mathrm{e} \times q_\mathrm{e}}, \\ \text{where} \quad q_\mathrm{amp} &= \frac{A}{G_\mathrm{preamp}} \\ \text{and} \quad N_\mathrm{e} &= \frac{\varepsilon_\mathrm{particle}}{W_{ij}}. \end{aligned} \tag{3}$$

Here, $\varepsilon_\mathrm{particle}$ is the energy deposited by some radiation inside the gas and W_{ij} is the average energy to produce an electron-ion pair in a mixture of the gases i and j, which makes N_e the number of electrons liberated by the incoming radiation. The charge after amplification in the gas, *i.e.* the input charge at the preamplifier is q_amp, A is the amplitude of a measured signal, and G_preamp denotes the preamplifier gain. The factor q_e is the electron charge. For the CREMAT amplifiers used in this work, $G_\mathrm{preamp} = 0.121\,\mathrm{mV\,pC^{-1}}$. W_{ij} needs to be calculated for each gas mixture, according to

$$W_{ij} = \left(\frac{f_i}{W_i} + \frac{f_j}{W_j} \right)^{-1} \quad . \tag{4}$$

Where f_i and f_j are the mixing fractions of each component of the mixture. For example, $W^{(90\text{-}10)}_{\text{Ar-}CO_2} = 26.6\,\mathrm{eV}$. The values for pure Ar, CO_2 and CH_4 are $W_\mathrm{Ar} = 26\,\mathrm{eV}$, $W_{CO_2} = 33\,\mathrm{eV}$, and $W_{CH_4} = 28\,\mathrm{eV}$, respectively [15].

The mean of the Gaussian function fitted to the photopeak, i.e. p_6 in Eq. (1) and p_3 in Eq. (2), is taken as the mean energy deposit of the x-ray emission from the ^{55}Fe source, that is A in Eq. (3). Hence, following the analysis in Section 3, G_OROC can be calculated for each anode voltage, pressure, and gas mixture. Table 1 shows the maximum stable voltages achieved in each gas mix and pressure, and the maximal G_OROC, denoted as G^max, measured at those settings. The OROC gas gain plotted as a function of voltage at each gas setting is shown in Figure 12.

At the same pressure and voltage settings, a much higher gas gain was measured with Ar-CH_4 than with Ar-CO_2. For example, in Ar-CO_2 (90-10) at 3 barA at $V_\mathrm{a} = 2675$ V, G_OROC was measured to be $(6.5 \pm 0.3) \times 10^3$.

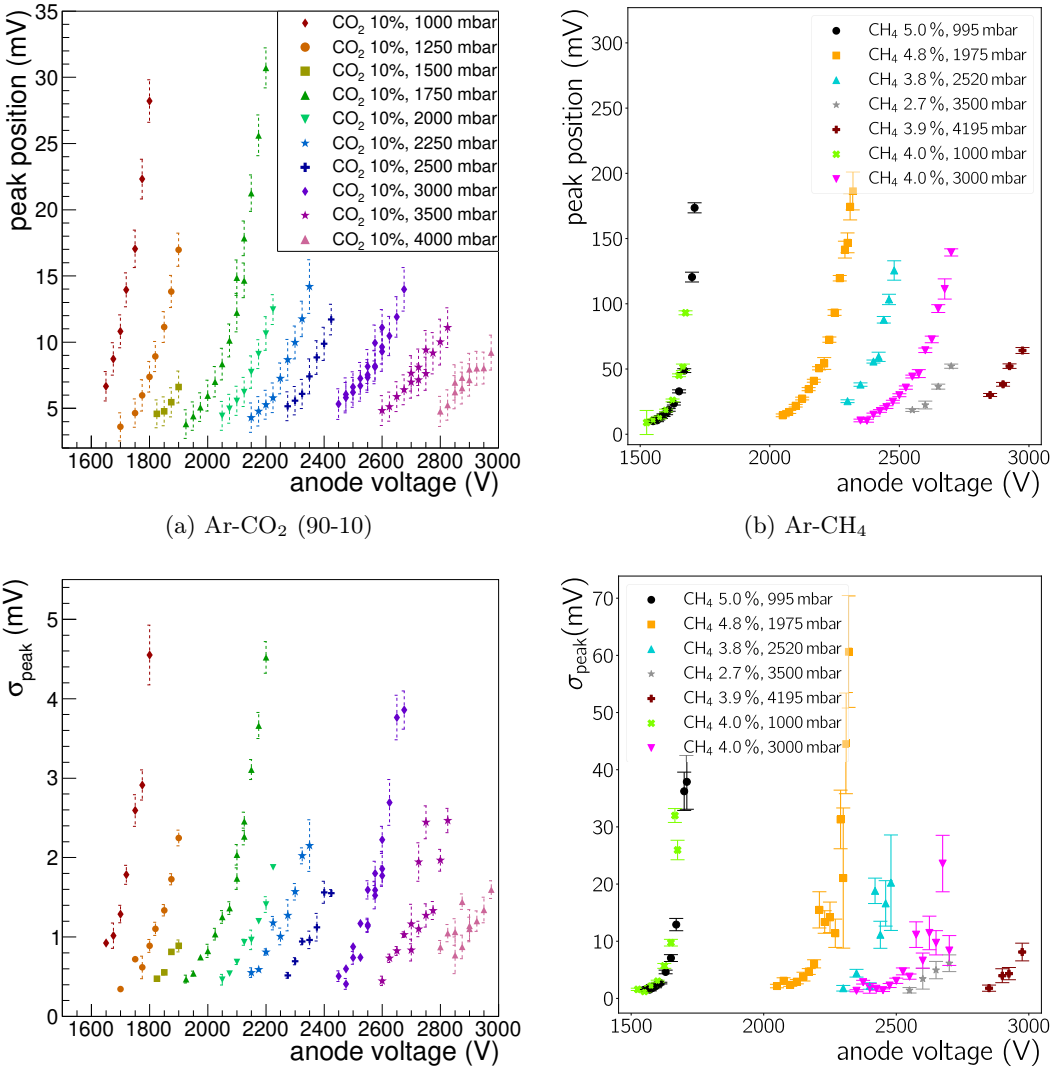

(a) Ar-CO_2 (90-10)

(b) Ar-CH_4

(c) Ar-CO_2 (90-10)

(d) Ar-CH_4

Figure 10: Fit results for fits of Eq. (1) and Eq. (2) to the Ar-CO_2 (90-10) (first column) and Ar-CH_4 (second column) data, respectively. In the first row, (a) and (b), the photopeak position (p_6 and p_3 in Eq. (1) and Eq. (2), respectively) is shown. The plots in the second row, (c) and (d), display the fit result for σ_{peak} (p_7 and p_4 in (1) and (2), respectively). The data was taken with the OROC using $V_{\text{gg}} = -143\,\text{V}$ and $V_{\text{d}} = -16\,\text{kV}$ ($E_{\text{d}} = -476\,\text{V}\,\text{cm}^{-1}$), whilst varying the anode voltage. An additional error of 1 mV is included to account for electronic noise in the readout removed by the smoothing algorithm. See Table 1 for the uncertainties on pressure values and mixing ratios.

For the same pressure and anode voltage in Ar-CH_4 (96-4), G_{OROC} was measured to be $(51\pm4)\times10^3$, a factor of 7.9 greater. Comparing the maximum gas gain measured with all Ar-CH_4 mixtures to Ar-CO_2 (90-10) of similar pressures, G^{max} was greater by a factor ranging from 5.5 ± 0.9 to 15 ± 2, and on average by a factor of 10.0 ± 0.6. This substantially greater gain when using the Ar-CH_4 mixtures is expected, considering the difference in quencher fraction and the resulting difference of the (effective) 1st Townsend coefficient in Ar-CH_4 mixtures with $\sim4\,\%$ CH_4 content compared to Ar-CO_2 (90-10) mixtures [16]. Gain simulations [11] and previous measurements [17] show a similar trend, although both are not directly comparable to the detector used for the measurements in this paper.

4.3 Extrapolation to pressure needed for a long-baseline experiment's ND

As expected, the measured gas gain increases exponentially with increasing anode voltage. The lines in the plots in Figure 12 are fits of the exponential function

$$G_{\text{OROC}}\left(V_{\text{a}}\right) = \text{e}^{m_{\text{exp}}^{\text{gain}}\left(V_{\text{a}} - b_{\text{exp}}^{\text{gain}}\right)}, \tag{5}$$

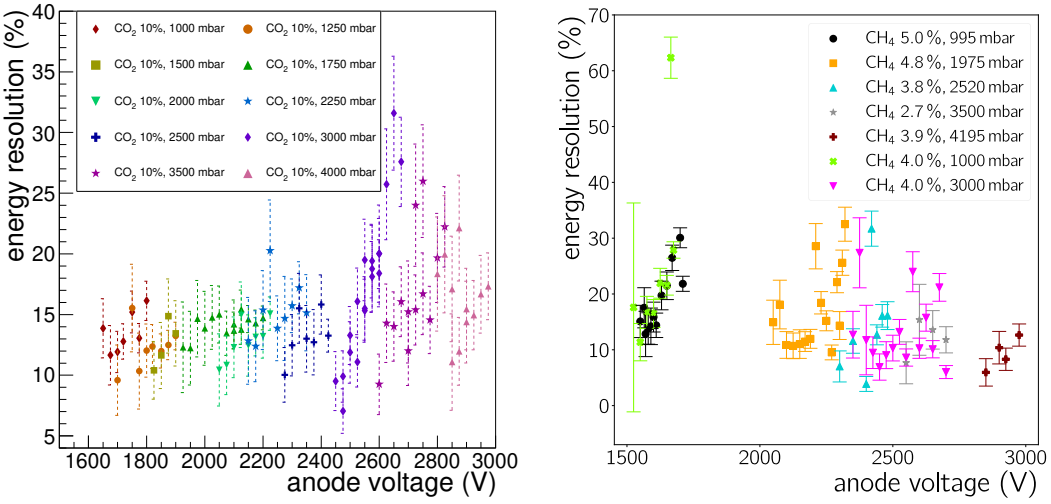

(a) Ar-CO_2 (90-10) (b) Ar-CH_4

Figure 11: Energy resolution ($\frac{\sigma_{\text{peak}}}{\text{peak position}}$) as function of anode voltage for data obtained with an ^{55}Fe source for (a) pressures between 1 barA and 4 barA in Ar-CO_2 (90-10), and (b) pressures between 1 barA and 4.8 barA in different Ar-CH_4 mixtures. This data was taken with the OROC using $V_{\text{gg}} = -143\,\text{V}$ and $V_{\text{d}} = -16\,\text{kV}$ ($E_{\text{d}} = -476\,\text{V cm}^{-1}$), whilst varying the anode voltage V_{a}.

Pressure (mbarA)	$V_{\text{a}}^{\text{min}}$ (V)	$V_{\text{a}}^{\text{max}}$ (V)	G^{max} $\times 10^3$	
1000	1650	1800	13.1 ± 0.7	
1250	1700	1900	7.9 ± 0.6	$\star$
1500	1825	1900	3.0 ± 0.5	$\star$
1750	1925	2125	6.8 ± 0.6	
2000	2050	2225	5.8 ± 0.5	
2250	2150	2350	6.6 ± 0.9	
2500	2275	2425	5.4 ± 0.5	
3000	2475	2600	4.3 ± 0.7	
3500	2600	2750	4.4 ± 0.7	
4000	2800	2875	3.4 ± 0.5	
1750	2100	2200	14.3 ± 0.7	
3000	2450	2600	5.2 ± 0.6	
3000	2550	2675	6.5 ± 0.8	
3500	2700	2825	5.2 ± 0.7	
4000	2850	2975	4.3 ± 0.6	

(a) Ar-CO_2 (90-10)

Pressure (mbarA)	$V_{\text{a}}^{\text{min}}$ (V)	$V_{\text{a}}^{\text{max}}$ (V)	f_{CH_4} (%)	G^{max} $\times 10^3$	
995	1400	1710	$5.0 \pm 0.5 \pm 0.1$	80 ± 2	
1975	1775	2320	$4.8 \pm 0.3 \pm 0.1$	85 ± 7	
2520	2225	2480	$3.8 \pm 0.2 \pm 0.1$	57 ± 3	
3500	2450	2700	$2.7 \pm 0.2 \pm 0.1$	24 ± 1	†
4195	2400	2975	$3.9 \pm 0.1 \pm 0.1$	29 ± 1	
4835	2700	2990	$4.1 \pm 0.1 \pm 0.1$	n.a.	
1000	1525	1675	$4.0 \pm 0.5 \pm 0.1$	42 ± 1	
3000	2300	2675	$4.0 \pm 0.2 \pm 0.1$	64 ± 1	
4420	2550	2975	$4.0 \pm 0.1 \pm 0.1$	n.a.	

(b) Ar-CH_4

Table 1: (a) All pressure settings for the Ar-CO_2 (90-10) measurements, and pressure and (b) gas mixture settings for the different Ar-CH_4 measurements with varying CH_4 fraction f_{CH_4}. The uncertainty on the pressure in (a) is ± 30 mbar and ± 5 mbar for the data in (b). The first uncertainty given for f_{CH_4} is due to this pressure uncertainty, whilst the second one arises because of the 0.2 % mixing uncertainty of the pre-mixed Ar-CH_4 and is fully correlated for all pressure settings. The range of anode voltages measured for each setting from the smallest ($V_{\text{a}}^{\text{min}}$) to largest ($V_{\text{a}}^{\text{max}}$) for all settings is given, too. For the settings marked by $\star$ in (a) a lower $V_{\text{a}}^{\text{max}}$ was used. The setting marked by † in (b) was not stable and the two settings reporting "n.a." as G^{max} had too low gain to discern the Fe spectrum. The horizontal line in each table splits two different periods of data taking with an evacuation of the vessel in-between.

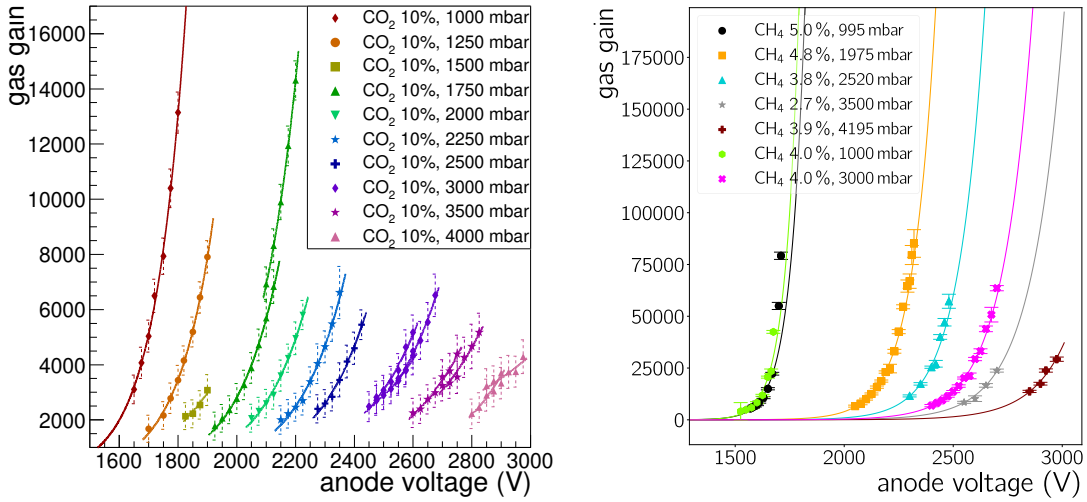

(a) Ar-CO_2 (90-10) (b) Ar-CH_4

Figure 12: Gas gain vs anode voltage for (a) pressures between 1 barA and 4 barA in Ar-CO_2 (90-10), and (b) pressures between 1 barA and 4.8 barA in different Ar-CH_4 mixtures. All data has been obtained with an ^{55}Fe source. This data was taken with the OROC using $V_{\mathrm{gg}} = -143\,\mathrm{V}$ and $V_{\mathrm{d}} = -16\,\mathrm{kV}$ ($E_{\mathrm{d}} = -476\,\mathrm{V\,cm^{-1}}$), whilst varying the anode voltage V_{a}. See Table 1 for the uncertainties on pressure values and mixing ratios.

where $m_{\mathrm{exp}}^{\mathrm{gain}}$ and $b_{\mathrm{exp}}^{\mathrm{gain}}$ are the slope and shift of the exponential, respectively. For both gas mixtures, the slope of the fits ($m_{\mathrm{exp}}^{\mathrm{gain}}$) decreases with increasing gas pressure. That is to say that in higher pressure gas mixtures we measure the gas gain to increase more slowly with increasing anode voltage.

A tonne-scale detector with the ALICE TPC's volume would need to operate at 10 barA pressure. By extrapolating $m_{\mathrm{exp}}^{\mathrm{gain}}$ and $b_{\mathrm{exp}}^{\mathrm{gain}}$ from the fits in Figure 12 to 10 barA pressure, we can comment on the OROC's suitability for operation as a long-baseline neutrino experiment ND with the gas mixtures examined in this paper. From the Eq. 5 fits to the Ar-CO_2 (90-10) data (Ar-CH_4 data), the anode voltage V_{a} at which $G_{\mathrm{OROC}} = 5000$ ($G_{\mathrm{OROC}} = 10000$), denoted as G_{5000} (G_{10000}), is interpolated. We deem these to be the sufficient values of G_{OROC} necessary to take a set of measurements with a similar range as those presented in Section 3. At such gain values, previous TPCs have performed tracking and particle ID of charged particles down to minimum ionizing particles, and contemporary readout electronics will be able to handle the corresponding charge inputs with ease [5]. Figure 13a and Figure 13b plot this voltage, $V_{\mathrm{a}}(G_{5000})$ ($V_{\mathrm{a}}(G_{10000})$), against pressure ($P$) for Ar-$CO_2$ (90-10) data (Ar-CH_4 data). These plots are fitted with the function

$$V_{\mathrm{a}}\left(G_i\right) = p_0 \cdot \ln\left\{\frac{P - p_1}{p_2}\right\}, \tag{6}$$

where i stands for 5000 or 10000 for Ar-CO_2 (90-10) and Ar-CH_4 data respectively. The fit is extrapolated to determine $V_{\mathrm{a}}(G_i)$ for higher pressures up to 10 barA. This extrapolation is less motivated for the Ar-CH_4 data than it is for the Ar-CO_2 (90-10), given that different mixing ratios are used for the first case. As these are mostly in the vicinity of $\sim$4 % CH_4, the approach detailed here should still yield a rough estimate for the $P = 10$ barA performance with such a mixture. Diethorn's formula [18] states that

$$\ln\left\{\frac{G_{\mathrm{OROC}}}{V_{\mathrm{a}}}\right\} \propto \ln\left\{\frac{V_{\mathrm{a}}}{P/P_0}\right\} \quad . \tag{7}$$

Choosing $P_0 = 1000$ mbarA, Figure 13c shows this linear relation for the measured Ar-CO_2 (90-10) data as well as for the V_{a} (G_{5000}) point extrapolated to $P = 10$ barA. In case of Ar-CH_4 (Fig. 13d) the measured $P = 1$ barA points do not line up well with the other measured points. Due to its large uncertainty the extrapolated point (V_{a} (G_{10000}), $P = 10$ barA) fits the other points' distribution. Given that all points should be for the same mixing ratio in order to obey the Diethorn formula, the overall distribution of points seems acceptable. A future measurement with the same CH_4 fraction at different pressures is needed to confirm the relation in Eq. (7) for this gas mixture.

For the target pressure of 10 barA, the extrapolations in Figure 13 predict $V_{\mathrm{a}}(G_{5000}) = 4600 \pm 500\,\mathrm{V}$ with Ar-CO_2 (90-10) and $V_{\mathrm{a}}(G_{10000}) = 3600 \pm 400\,\mathrm{V}$ with similar Ar-CH_4 mixtures. The additional linear fit to the points in Figure 13c predicts $V_{\mathrm{a}}(G_{5000}) = 4400 \pm 500\,\mathrm{V}$ at the target pressure of 10 barA with Ar-CO_2 (90-10), consistent with the extrapolation in Figure 13a. These predicted values of V_{a} are above the range of voltages at which the OROC has currently been tested, so an operation of the OROC at 10 barA may not be possible at a sufficient gas gain in neither Ar-CO_2 (90-10) nor Ar-CH_4 with $\sim$4 % CH_4 content. However, if the upper limit for V_{a} is studied, and the OROCs can be safely operated with V_{a} larger than 3000 V, then sufficient gain may be achievable at 10 barA with these mixtures.

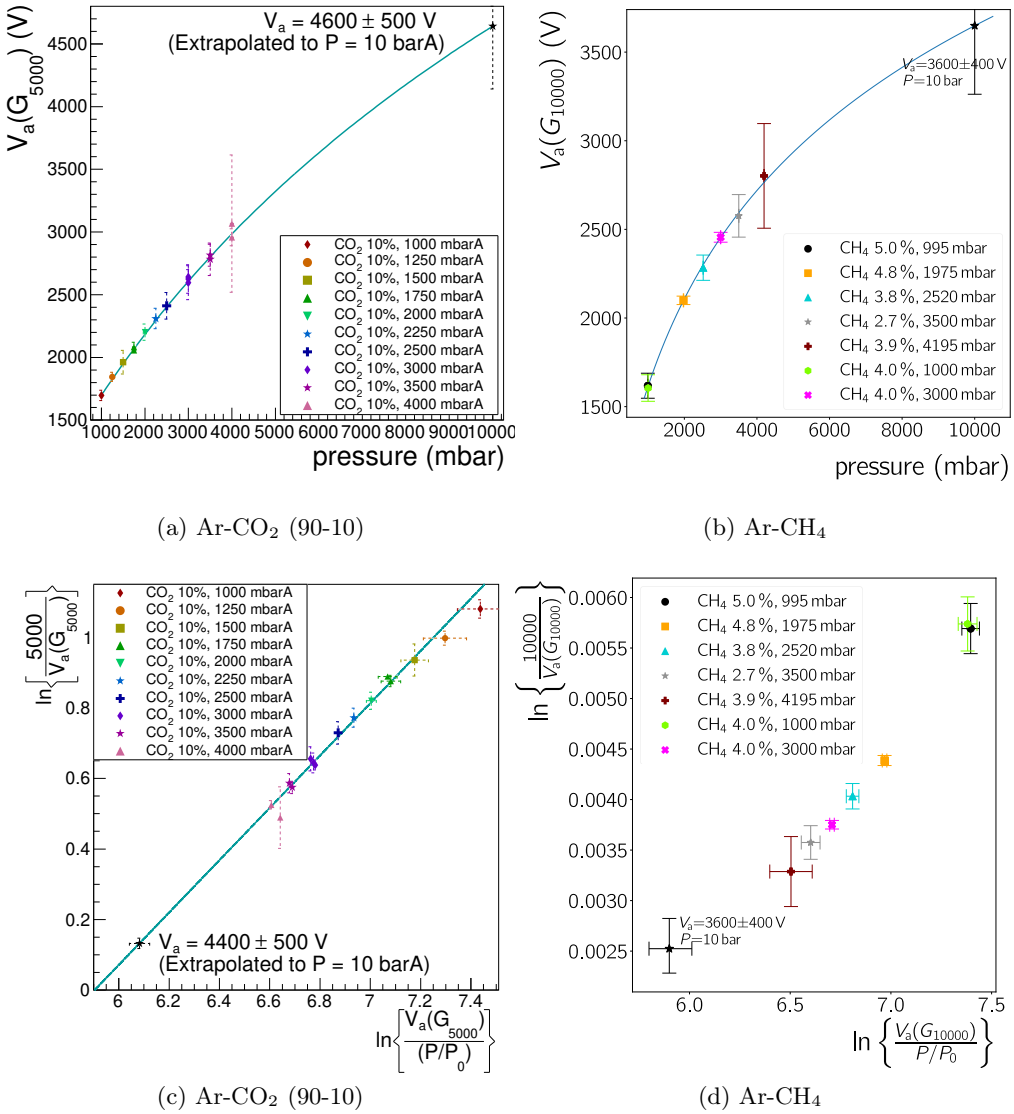

(a) Ar-CO_2 (90-10)

(b) Ar-CH_4

(c) Ar-CO_2 (90-10)

(d) Ar-CH_4

Figure 13: Extrapolation of the results from this paper to the tonne-scale detector design pressure of 10 barA. The first row plots $V_a(G_{5000})$ ($V_a(G_{10000})$) *i.e.* the voltage at which we measure a gain of 5000 (10,000), against pressure for data taken with (a) Ar-CO_2 (90-10) and (b) Ar-CH_4 mixtures. In each plot, a fit to the data following Eq. (6) extrapolates to pressures up to 10 barA, the extrapolated point at 10 barA and the corresponding values of V_a are indicated in each plot. The second row plots the Diethorn relation (Eq. 7) for (G_{5000}) ((G_{10000})) for the same data, (c) Ar-CO_2 (90-10) and (d) Ar-CH_4. The Ar-CO_2 (90-10) data points are fitted with a linear fit and extrapolated to predict a value for $V_a(G_{5000})$ at 10 barA of 4400 ± 500 V. Since several different mixing ratios were used, the Diethorn plot for the Ar-CH_4 data is not fitted. Instead, the extrapolated point at 10 barA from (b) is included in (d). See Table 1 for the uncertainties on pressure values and mixing ratios.

5 Summary and conclusion

A high pressure gas TPC is a good candidate to measure neutrino interactions for future long-baseline neutrino experiments such as the DUNE and HK experiments currently under construction in the United States and Japan, respectively. The ALICE detector has been recently upgraded [5] so the existing MWPCs from its pre-upgrade TPC are available as potential readout chambers for such a detector. These MWPCs were however only operated at atmospheric pressure.

The results presented here demonstrate for the first time the operation of an ALICE outer readout chamber (OROC) at pressures up to 4.2 barA in Ar-CH_4 mixtures with a CH_4 content between 2.8 % and 5.0 %, and up to 4 barA in Ar-CO_2 (90-10). In 4.2 barA Ar-CH_4 (96.1-3.9) (0.2 uncertainty on the mixture), a maximum gain of $(29\pm 1)\cdot 10^3$ was achieved with an anode wire voltage of 2975 kV and in 4 bar Ar-CO_2 (90-10) a gain of $(4.2 \pm 0.1) \cdot 10^3$ was observed with an anode voltage of 2975 V.

To achieve a tonne-scale neutrino target in a TPC of the volume of ALICE, a pressure of 10 barA would be required. We extrapolate that the OROC anode voltages required to make reasonable gain measurements at this target pressure are $V_a = 4600 \pm 500\,V$ ($V_a = 4400 \pm 500\,V$) with Ar-CO_2 (90-10) and $V_a = 3600 \pm 400\,V$ with an Ar-CH_4 mixture with $\sim 4\,\%$ CH_4. The latter value is less well extrapolated, as not all Ar-CH_4 mixtures in the calculation had the same CH_4 content. The Diethorn relation (Eq. (7)) states that the relationship between $\ln\{\frac{G_{OROC}}{V_a}\}$ and $\ln\{\frac{V_a}{P/P_0}\}$ should be linear and our measurements with Ar-CO_2 are consistent with this relationship. The Ar-CH_4 measurements also seem to follow the general trend, but a dedicated measurement with the same CH_4 fraction at all pressures is needed to confirm the relationship.

The so identified V_a for operation at 10 barA are above the maximal anode voltage at which the OROC has been tested, so an operation of the OROC at 10 barA may not be possible with sufficient gas gain in either Ar-CO_2 (90-10) or Ar-CH_4 with $\sim 4\,\%$ CH_4 content. Studies to determine a higher upper limit for V_a may be necessary. If V_a larger than 3000 V would be deemed to be safe for the wire chambers then, in Ar-CH_4 in particular, it may be possible to achieve higher pressures at reasonable gain values with the gas mixtures tested in this paper. The maximal V_a achievable without damage to the readout chambers has not been investigated and the limit of 3 kV used here is imposed as a precaution to protect the equipment while the maximum safe V_a is still unknown. The maximum pressure was limited by the rating of the UK high pressure platform [9], which can be operated only at pressures up to 5 barA. Other groups in the US are carrying out tests with a smaller inner ROC of the ALICE TPC at test-stand [19] that will be able to reach 10 barA.

Several optimisations could improve our results. The energy resolution for these measurements is generally between 10 % and 20 %, but we obtained values as high as 60 % for the highest pressure Ar-CH_4 measurements. This could be improved with better noise reduction and with more precise positioning of the ^{55}Fe source in the vessel, neither of which were optimised. The energy resolution can likely also be improved with better background subtraction at the analysis stage. Optimizations to improve energy resolution will become increasingly important for future studies, which are in preparation right now. Custom readout electronics based on the SAMPA chip are close to being finalised and will be tested in the near future; single pad readout and charge pre-amplification close to the pads will yield a better energy resolution and also allow for particle tracking.

References

[1] S. Manly and M. Kordosky on behalf of the DUNE Collaboration. 'Deep Underground Neutrino Experiment (DUNE) Near Detector Conceptual Design Report'. In: *Instruments* 5.4 (Sept. 2021), p. 31. ISSN: 2410-390X. DOI: 10.3390/instruments5040031.

[2] L. Alvarez-Ruso et al. 'NuSTEC1 1Neutrino Scattering Theory Experiment Collaboration http://nustec.fnal.gov. White Paper: Status and challenges of neutrino–nucleus scattering'. In: *Progress in Particle and Nuclear Physics* 100 (2018), pp. 1–68. ISSN: 0146-6410. DOI: https://doi.org/10.1016/j.ppnp.2018.01.006.

[3] M. A. Acero et al. 'Improved measurement of neutrino oscillation parameters by the NOvA experiment'. In: *Phys. Rev. D* 106 (3 2022), p. 032004. DOI: 10.1103/PhysRevD.106.032004.

[4] T. T. Collaboration et al. 'Measurements of neutrino oscillation parameters from the T2K experiment using 3.6×10^{21} protons on target'. In: (2023). arXiv: 2303.03222 [hep-ex].

[5] J. Alme et al. 'The ALICE TPC, a large 3-dimensional tracking device with fast readout for ultra-high multiplicity events'. In: *Nuclear Instruments and Methods in Physics Research Section A: Accelerators, Spectrometers, Detectors and Associated Equipment* 622.1 (2010), pp. 316–367. ISSN: 0168-9002. DOI: https://doi.org/10.1016/j.nima.2010.04.042.

[6] J. Adolfsson et al. 'The upgrade of the ALICE TPC with GEMs and continuous readout'. In: *Journal of Instrumentation* 16.03 (Mar. 2021), P03022. DOI: 10.1088/1748-0221/16/03/p03022.

[7] The ALICE Collaboration et al. 'The ALICE experiment at the CERN LHC'. In: *Journal of Instrumentation* 3.08 (Aug. 2008), S08002–S08002. DOI: 10.1088/1748-0221/3/08/s08002.

[8] B. B. Abelev et al. 'Performance of the ALICE Experiment at the CERN LHC'. In: *Int. J. Mod. Phys. A* 29 (2014), p. 1430044. DOI: 10.1142/S0217751X14300440. arXiv: 1402.4476 [nucl-ex].

[9] A. Deisting et al. 'Commissioning of a High Pressure Time Projection Chamber with Optical Readout'. In: *Instruments* 5.2 (2021). ISSN: 2410-390X. DOI: 10.3390/instruments5020022.

[10] *CR-112-R2.1 charge sensitive preamplifier: application guide*. 2018.

[11] S. Biagi. 'Magboltz 2'. In: *CERN computer newsletter No.2000-001 in section 'Scientific Applications and Software Engineering'* (Apr. 2000).

[12] I. Smirnov. 'Modeling of ionization produced by fast charged particles in gases'. In: *Nuclear Instruments and Methods in Physics Research Section A: Accelerators, Spectrometers, Detectors and Associated Equipment* 554.1 (2005), pp. 474–493. ISSN: 0168-9002. DOI: https://doi.org/10.1016/j.nima.2005.08.064.

[13] M. Berger et al. *XCOM: Photon Cross Sections Database, NIST Standard Reference Database 8 (XGAM)*. URL: https://www.nist.gov/pml/xcom-photon-cross-sections-database.

[14] M. L. Knichel. 'Characterization of a fully equipped ALICE TPC Readout Chamber'. May 2009.

[15] H. Kolanoski and N. Wermes. *Teilchendetektoren*. Springer, 2016.

[16] A. Deisting. 'Commissioning of a hybrid readout TPC test set-up and gas gain simulations'. In: *Journal of Physics: Conference Series* 2374.1 (Nov. 2022), p. 012145. DOI: 10.1088/1742-6596/2374/1/012145.

[17] A. Sharma and F. Sauli. 'First Townsend coefficient measured in argon based mixtures at high fields'. In: *Nuclear Instruments and Methods in Physics Research Section A: Accelerators, Spectrometers, Detectors and Associated Equipment* 334.2 (1993), pp. 420–424. ISSN: 0168-9002. DOI: https://doi.org/10.1016/0168-9002(93)90802-0.

[18] W. Blum, W. Riegler and L. Rolandi. *Particle Detection with Drift Chambers*. Springer-Verlag, 2008.

[19] T. A. Mohayai. 'A Gaseous Argon-Based Near Detector for DUNE'. In: *CPAD Workshop, Stony Brook University* (2022). DOI: https://doi.org/10.2172/1906054.